Proceedings of the
Annual Stability Conference
Structural Stability Research Council
St. Louis, Missouri, April 2-5, 2019

Large-scale lateral–torsional buckling tests of welded girders

Xiao Lin Ji[1], Robert G. Driver[2], Ali Imanpour[3]

Abstract
Currently, the Canadian steel design standard, CAN/CSA S16-14, prescribes unified design equations for predicting lateral–torsional buckling that do not distinguish between rolled and welded sections. However, residual stresses present in welded sections can create unfavourable conditions that may reduce their resistance to lateral–torsional buckling. Recent numerical studies reinforce this notion and have indicated that the current design equations to determine lateral–torsional buckling resistance may be unconservative for welded girders, particularly in the inelastic range. Despite the numerical evidence, there is a paucity in up-to-date physical testing of welded girders fabricated with modern processes, which forms a substantial gap when concluding the adequacy of CSA S16-14. This paper discusses the lateral–torsional buckling physical testing program being undertaken at the University of Alberta Steel Centre. Development of the unique girder-stability test-bed is described and preliminary results of the first large-scale specimen, 9.75 m (32 ft) in length and with laterally and torsionally pinned end conditions, are presented.

1. Introduction

Lateral–torsional buckling (LTB) is a potential failure mode of unbraced steel beams wherein a member undergoes coupled lateral movement and twisting under a major axis flexural bending moment. This failure occurs when sections have much greater stiffness about the plane of loading (major axis) than about their minor axis. If members are insufficiently braced, LTB may occur before they attain their full cross-sectional flexural capacity. In Canada, LTB provisions are determined in accordance with the Canadian steel design standard CAN/CSA S16-14 (CSA 2014). Three separate but related equations, as defined in Eqs. 1-4, form the beam design curve where LTB is implicitly included as a limit state. The curve identifies three ranges of behaviour: elastic buckling, inelastic buckling, and cross-sectional capacity.

$$If\ M_u > 0.67M_p: \quad M_r = 1.15\phi M_p \left[1 - \frac{0.28M_p}{M_u}\right] \leq \phi M_p \tag{1}$$

$$If\ M_u \leq 0.67M_p: \quad M_r = \phi M_u \tag{2}$$

[1] Master of Science Student, University of Alberta, <xlji@ualberta.ca>
[2] Professor, University of Alberta, <rdriver@ualberta.ca>
[3] Assistant Professor, University of Alberta, <imanpour@ualberta.ca>

$$M_u = \frac{\omega_2 \pi}{L} \sqrt{EI_y GJ + \left(\frac{\pi E}{L}\right)^2 I_y C_w} \tag{3}$$

$$\omega_2 = \frac{4M_{max}}{\sqrt{M_{max}^2 + 4M_a^2 + 7M_b^2 + 4M_c^2}} \leq 2.5 \tag{4}$$

where M_r is the factored moment resistance, ϕ is the resistance factor, M_p is the plastic moment capacity of the section, M_u is the critical elastic moment of the unbraced segment, ω_2 is the moment gradient coefficient, L is the length of the unbraced segment of the beam, E is the modulus of elasticity, I_y is the moment of inertia about the minor principal axis, G is the shear modulus of elasticity, J is the St. Venant torsional constant, C_w is the warping torsional constant, M_{max} is the maximum factored moment in the unbraced segment, and M_a, M_b, M_c are the factored moments at one-quarter point, midpoint, and three-quarter point of the unbraced segment, respectively.

Currently, the beam curve does not distinguish between rolled and welded girders despite their distinctly different residual stress distributions (MacPhedran and Grondin 2011). However, there is a known correlation between residual stresses and LTB, which raises the question—is it necessary to differentiate LTB resistance for rolled and welded shapes, particularly in the inelastic region where residual stresses become significant? While recent studies have suggested that the current CSA S16-14 provisions may be unconservative for welded sections (Kabir and Bhowmick 2018; MacPhedran and Grondin 2011), it is important to separate previous LTB research into two broad groups: physical testing and numerical analysis. Most physical testing on welded sections was conducted in the 1970s and 1980s in Japan (Fukumoto 1976; Fukumoto et al. 1980; Fukumoto and Itoh 1981); the studies raising concerns with CSA S16-14 are far more recent and fall under numerical analysis (MacPhedran and Grondin 2011; Kabir and Bhowmick 2016). Fabrication and welding processes change and improve over time, which influence initial imperfections, residual stresses, and therefore LTB resistance. If numerical studies are corroborated against an outdated database of tests, it is difficult to conclude whether current design provisions are truly inadequate. Given the ubiquity of unbraced beams and girders in structural applications, there is an urgent need for physical tests on modern welded sections before conclusions regarding the adequacy of CSA S16-14 can be drawn.

This paper discusses an experimental test program on welded steel girders at the University of Alberta CISC Centre for Steel Structures Education and Research (Steel Centre). A review of previous studies is first presented, then development of the unique girder-stability test-bed is discussed, particularly the loading mechanism. Finally, preliminary test results from the first girder test are presented.

2. Overview of past research

Studies of LTB began with simple cases of elastic buckling (Timoshenko and Gere 1961) and strong confidence in the analytical solutions have yielded a simplified design approach for elastic lateral stability of continuous beams (Galambos 1977). However, inelastic LTB poses challenges as it is difficult to characterize the extent of yielding and the deterioration of relevant stiffness parameters (Galambos 1977, 1998). Moreover, residual stresses play a pertinent role as deviation

from elastic behaviour can depend heavily on the amplitude and distribution of compressive residual stresses in the compression flange (Galambos 1977). The correlation between residual stresses and LTB then raises the question for distinguishing between rolled and welded girders, as they have significantly different residual stress distributions. In Fukumoto's (1976) tests on 36 annealed and welded beams and girders, he concluded that residual stresses in welded sections reduced their resistance to LTB. Further studies by Fukumoto and Kubo (1977) indicated that, for 156 rolled and 112 welded beam tests, welded beams exhibited larger scatter and lower lateral buckling capacity than rolled beams. MacPhedran and Grondin's (2011) study echoed this conclusion and they proposed a simplified beam equation that distinguishes between rolled and welded sections. Using test data from Greiner and Kaim (2001), they conducted a statistical evaluation comparing CSA S16-09's LTB provisions and their proposed equation. From the 144 tests on rolled shapes and 71 tests on welded sections, they concluded that CSA S16-09 achieves the desired reliability index of 3.0 for rolled sections but only yields 1.6 for welded sections when using the prescribed resistance factor of 0.9. Kabir and Bhowmick (2016; 2018) reaffirmed MacPhedran and Grondin's (2011) findings through numerical simulations that show CSA S16-14 may be unconservative for welded girders in the inelastic range. However, Subramanian and White (2017) observed that numerical models often yield lower capacities than test results and design equations, which may be attributed to assuming overly conservative initial imperfections and residual stress distributions.

3. Experimental test program

As a response to the paucity in up-to-date physical test data, the Steel Centre at the University of Alberta has launched an LTB testing program of large-scale welded girders. Girder capacity is obtained and compared against current CSA S16-14 provisions, with the intent to examine CSA S16-14's adequacy for predicting LTB resistance in welded steel girders. The test program involves 11 tests focused on the inelastic LTB range, which has been identified as an area of concern (Galambos 1977). All girders are fabricated with welding and manufacturing processes typical of today's industry. Detailed residual stress measurements of all test girders are recorded in a companion project (Unsworth et al. 2019).

3.1 Test configuration

The proposed test involves 9.75 m long girders that rest on roller supports to ideally achieve symmetrical deformations about the girder centreline. Eight equally-spaced concentrated loads, *P*, are applied to the top flange of the girder, as shown in Fig. 1. The girder is torsionally pinned at the supports; no lateral bracing is provided along the span.

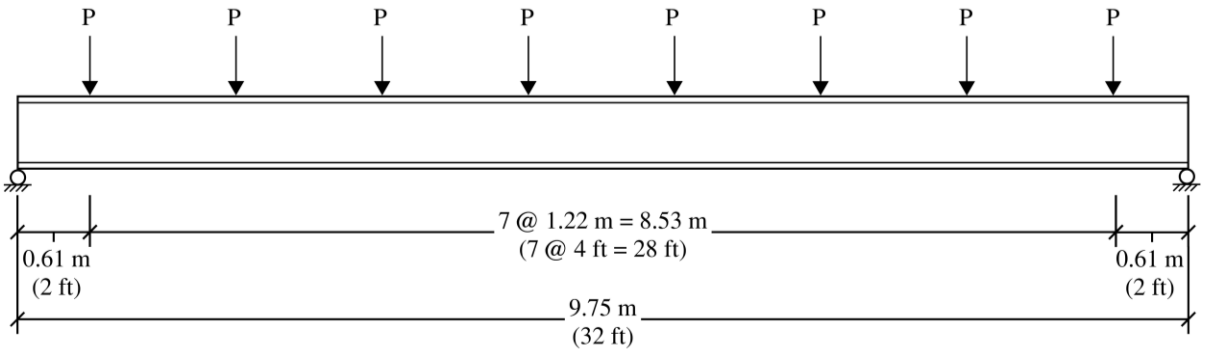

Figure 1: Load configuration.

3.2 Test matrix

The test matrix shown in Table 1 considers nine unique girder cross-sections and 11 specimens in total, where *w* is web thickness, *d* is section depth, *b* is flange width, and *t* is flange thickness. As plate cutting is shown to have a significant effect on residual stress distribution (Ballio and Mazzolani 2013), SP2 and SP7 are fabricated by both flame cutting and plasma cutting; the sections are otherwise identical and thus the effect of cutting method on LTB resistance can be ascertained. Other criteria considered in the test matrix include: allowance for comparison of *b* and *t*, aspect ratio (*d/b*), range of inelastic behaviour, and section class (compact vs. non-compact).

Table 1: Test girder matrix

No.	Serial No.[1]	Total Qty	w^2 (mm)	d (mm)	b (mm)	t^3 (mm)	d/b
SP1	G6-470-32-2-p	1	12.7	600	470	31.75	1.28
SP2-1	G6-430-32-1-p	2	12.7	600	430	31.75	1.40
SP2-2	G6-430-32-1-f						
SP3	G6-300-32-1-p	1	12.7	600	300	31.75	2.00
SP4	G8-430-25-2-p	1	12.7	800	430	25.4	1.86
SP5	G8-390-32-2-p	1	12.7	800	390	31.75	2.05
SP6	G8-390-25-2-p	1	12.7	800	390	25.4	2.05
SP7-1	G9-360-32-3-p	2	9.525	900	360	31.75	2.50
SP7-2	G9-360-32-3-f						
SP8	G9-360-25-3-f	1	9.525	900	360	25.4	2.50
SP9	G9-430-25-3-f	1	9.525	900	430	25.4	2.09

1. Serial number name convention is ‘G’ followed by: first digit of section depth – flange width – flange thickness – class – cutting method (‘p’ for plasma, ‘f’ for flame)
2. 9.525 mm and 12.7 mm web thicknesses correspond to 0.375 in and 0.5 in, respectively
3. 25.4 mm and 31.75 mm flange thicknesses correspond to 1 in and 1.25 in, respectively

3.3 Test set-up

As a failure mode, LTB inherently involves a multitude of movement; the girder is expected to displace longitudinally, bend about the major and minor axes, and rotate. The test set-up must therefore accommodate all expected displacements and rotations without restraint. A schematic model of the final test set-up is shown in Fig. 2.

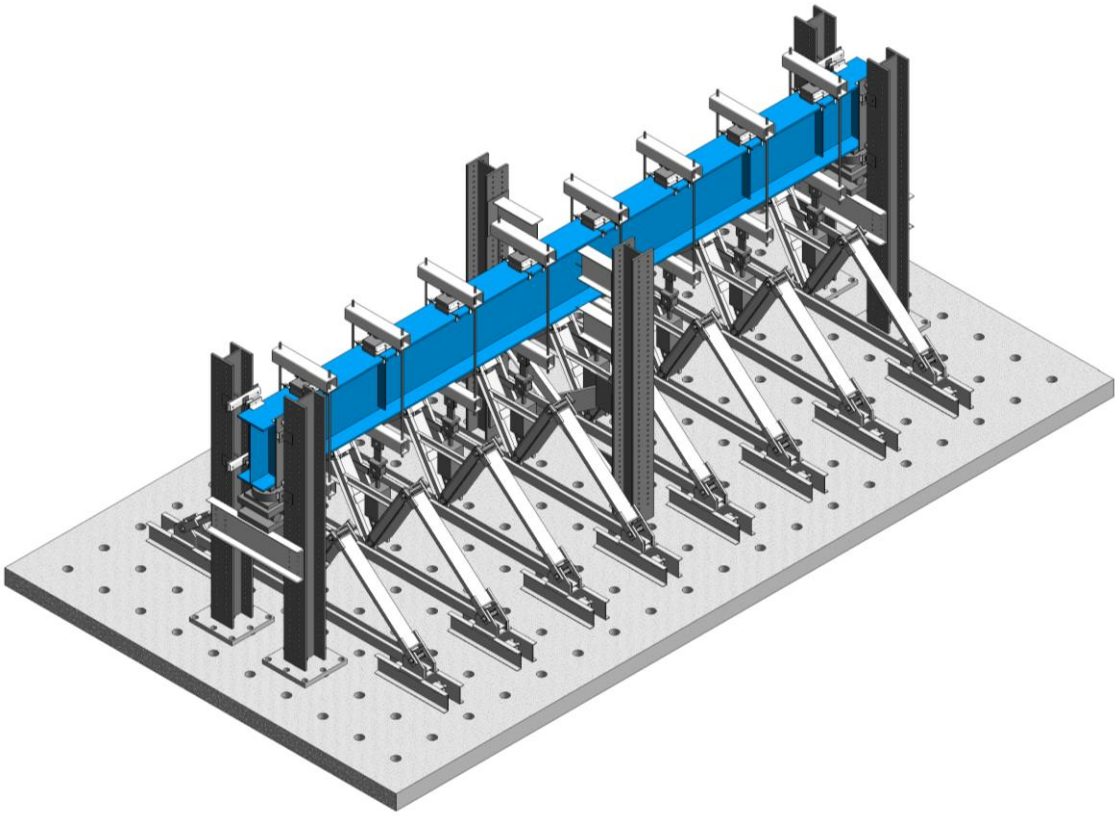

Figure 2: Test set-up (girder shown in blue is SP9)

3.3.1 Preliminary finite element model

To anticipate the expected displacements and rotations in the test, non-linear finite element analyses for all test girders were conducted using Abaqus (Dassault Systèmes 2014). Three-dimensional shell elements (S4R) were used to model the sections. A mesh size of 25.4 mm was chosen, which amounts to 12 – 16 elements across the flange and 22 – 34 elements in the web for the proposed test specimens. The material was assumed to be elastic-perfectly plastic with a yield stress of 385 MPa, modulus of elasticity of 200 000 MPa, and Poisson's ratio of 0.3.

The purpose of the finite element analysis (FEA) was to develop a numerical model capable of providing preliminary pre-test predictions of buckling load, displacements, and rotations, which allows for improved design of the test set-up. An eigenvalue buckling analysis was first conducted to obtain the elastic buckling modes, including LTB mode shapes, which was then used as the initial geometric out-of-straightness pattern in the subsequent non-linear RIKS analysis. While CSA G40.20-13 (CSA 2013a) indicates $L/500$ for geometric out-of-straightness, where L is the

unbraced length of the member, CSA W59-13 (CSA 2013b) has a stricter requirement of $L/1000$. Therefore, the maximum imperfection value, located at mid-span, is scaled to $L/1000$ in the finite element model. For simplicity, no residual stresses were included.

Pertinent movements were recorded for all girders, including the following:

1. Lateral displacement at compression (top) flange tip
2. Vertical displacement at tension (bottom) flange centroid
3. Twist of top flange, measured at flange centroid
4. Longitudinal displacement at bottom flange centroid at both boundary conditions

The first three are particularly important to consider for the load mechanism design, as discussed in the subsequent section.

3.3.2 Load application

The finalized loading mechanism, as shown in Fig. 3, consists of three components: (1) a load collar, (2) a hydraulic actuator, and (3) a gravity load simulator. The gravity load simulator is a pin-jointed apparatus designed for testing specimens that sway (Yarimci et al. 1967); it is capable of moving laterally while maintaining close-to-vertical load application. The gravity load simulator is connected to the hydraulic actuator, which is then attached to a load collar that wraps around the girder. Combined, the three components must accommodate vertical displacement, lateral movement, and cross-section rotation of the girder at each load point. The fabricated load mechanism is shown in Fig. 4.

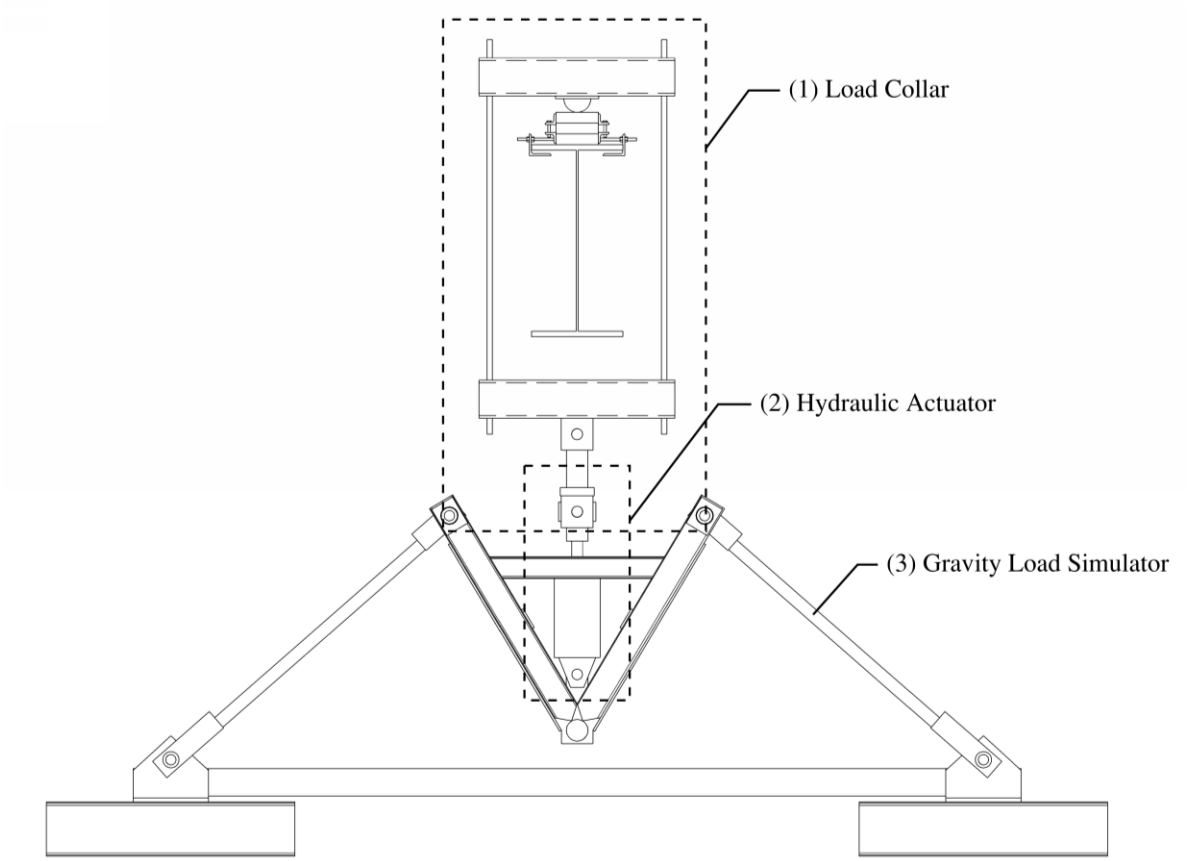

Figure 3: Components of the load mechanism (at each load point)

Figure 4: Gravity load mechanism

At the beginning of the test, the hydraulic actuator is fully extended; as it retracts, it pulls on the load collar, which applies a downward concentrated load on the test girder. The vertical displacement of the girder is therefore accommodated by the retracting stroke of the hydraulic actuator. The load collar is designed to remain elastic with large rigidity compared to the test specimen; rollers are provided to allow for slight longitudinal movement of the girder as the system initially self-aligns and a rotational hemisphere is used to accommodate girder twist. The point of rotation is therefore at the contact point between the hemisphere and the roller, which effectively means the girder is loaded above its top flange. Lastly, lateral movement of the girder is unrestrained as the gravity load simulator sways to accommodate the out-of-plane buckling while continuously applying vertical load. The design capacity of the gravity load simulator is 380 kN but it shall not be operated beyond 360 kN as an extra margin of safety (Ji et al. 2018). The remaining components of the loading mechanism are therefore designed to remain elastic up to 360 kN. All test girders have been designed to fail in inelastic LTB with 360 kN or less applied at each of the eight load points. The maximum movements at buckling from the finite element analyses are used to ensure the load mechanism contains sufficient displacement and rotational capacity, as summarized in Table 2. A large safety margin is provided between expected movements at buckling and allowable movement in the load mechanism as post-buckling displacements and rotations are desired. Moreover, instability is inherently difficult to predict.

Table 2: Displacement and rotation demands at load points

	Maximum mid-span movement at buckling from FEA	Allowable movement in designed load mechanism	Corresponding component of load mechanism
Vertical displacement	57.0 mm	150 mm	Stroke of hydraulic actuator
Horizontal displacement	73.1 mm	140 – 225 mm[1]	Gravity load simulator[1]
Twist	6.01°	10.0°	Rotational hemisphere

1. The gravity load simulator can sway up to 400 mm in either direction but this amount of movement is deemed unsafe and therefore safety stops are installed to cap horizontal displacement at 140 mm (for the widest flange) to 225 mm (for the narrowest flange)

3.3.3 Lateral bracing at end supports

To achieve torsionally pinned boundary conditions, four lateral braces at each end support are used, as shown in Fig. 5. The braces are designed to bear against the top and bottom flange tips to prevent lateral movement and twist but are also equipped with rollers that allow the girder to move longitudinally and warp. To give the rollers a larger bearing area, side plates that hang off either side of the girder are used. Furthermore, the use of threaded rod in the design allows for adjustability in the overall length of the brace, which serves a three-fold purpose: (1) to ensure the brace firmly bears against flange tips, (2) to align the girder so that its web sits vertical at end supports, and (3) to accommodate various flange widths.

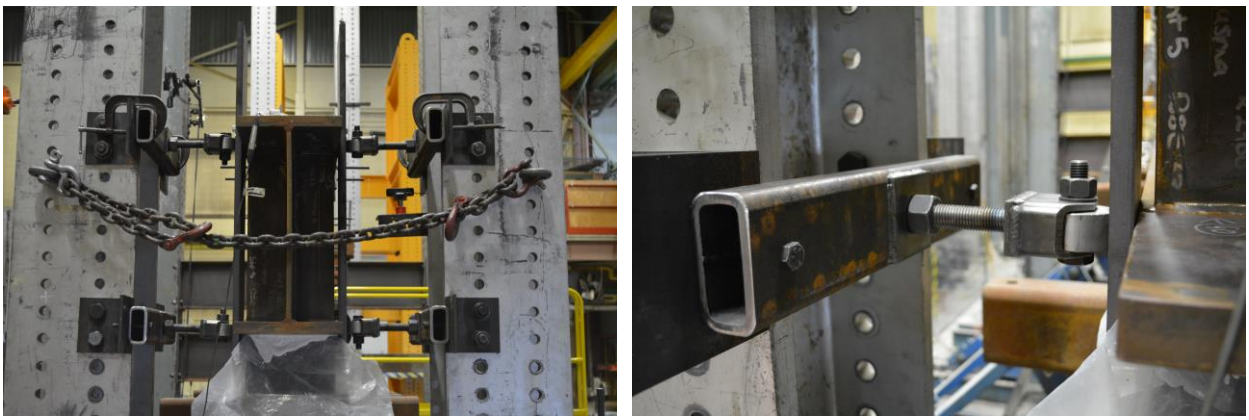

Figure 5: Lateral braces at end support (left) and a close-up view of an individual brace (right)

4. Test results

Results of the first test on SP2-2 are hereon presented. Residual stresses for SP2-2 were measured through sectioning methods by Unsworth et al. (2019).

4.1 Initial geometric imperfections

Cross-section imperfections and global geometric imperfections such as lateral out-of-straightness (sweep), camber, and twist are measured at five points along the girder. Fig. 6 indicates the location of the five points where Point 1 is considered the north end of the girder and Point 5 is considered the south end.

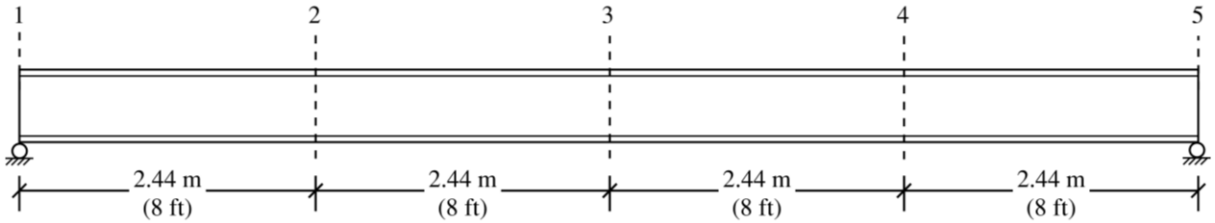

Figure 6: Initial geometric imperfection measurement locations along the specimen.

Table 3 summarizes the cross-section imperfections for SP2-2 while Fig. 7 depicts the out-of-straightness imperfection measurements.

Table 3: Nominal vs. measured cross-section dimensions of SP2-2

	d (mm)	*b* (mm)	*t* (mm)	*w* (mm)
Nominal	600	430	31.75	12.7
Measured	591	422	32.16	13.1

Sweep and camber are measured at the top and bottom flanges while the girder is on the working surface on the laboratory strong floor. Once the girder is lifted into the test set-up, the girder web at both end supports is aligned to 90°, which corresponds to 0° twist; the corresponding twist at Points 2, 3, and 4 is then measured. Results of the measurements showed that top flange sweep is approximately *L*/3200 as compared to the *L*/1000 tolerance allowed by CSA W59-13. Maximum twist of the web is measured to be 0.25° and maximum camber is -6.25 mm at the top flange, where negative camber corresponds to positive bending.

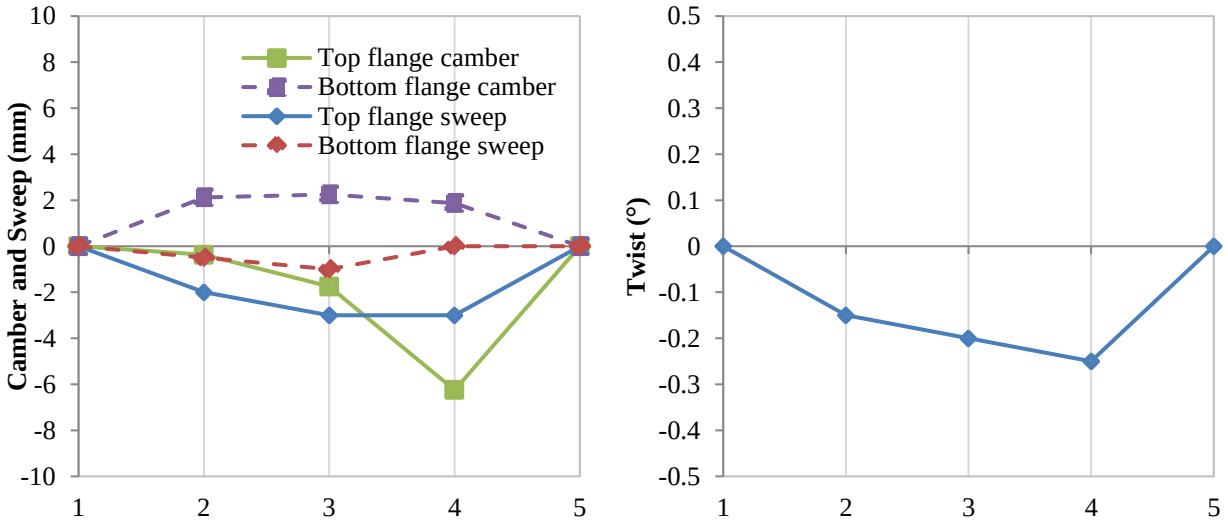

Figure 7: Initial out-of-straightness measurements for SP2-2

4.2 Global response and test observation

The vertical load versus mid-span lateral and vertical displacement curves for SP2-2 from test results are shown in Fig. 8, where the load, P_{avg}, represents the average force applied at eight load points. Further displacements and rotations from the test at buckling and at their maximum attained value (i.e. at the end of the test, immediately before unloading) are provided in Table 4, which serves to provide additional insight into the response of SP2-2.

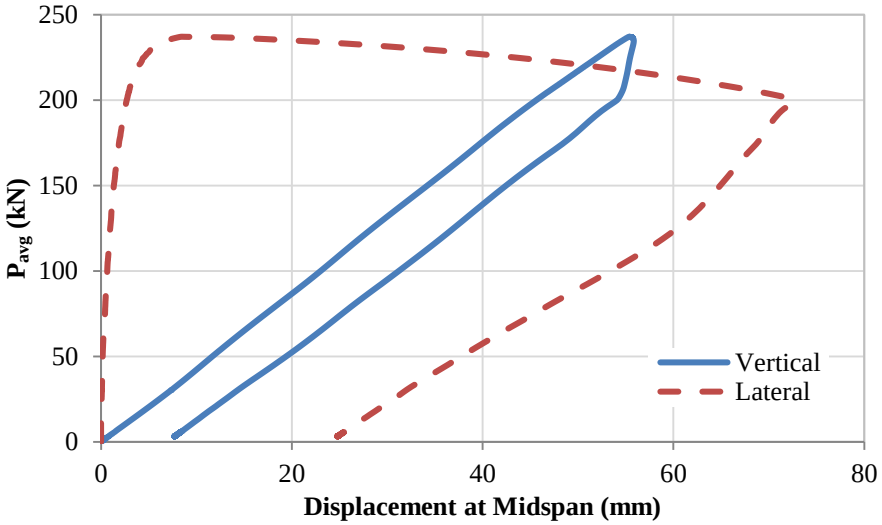

Figure 8: Load vs. displacement at mid-span of SP2-2

Specimen SP2-2 reached an experimental peak or buckling load of $P_{avg} = 237$ kN, which corresponds to a moment capacity of *2313* kN-m. The general girder behaviour observed was consistent with what is expected in an LTB failure. Prior to reaching the buckling load, very little lateral displacement was measured. Upon buckling, the girder's strength slowly dropped as top flange lateral displacement increased rapidly, from 8.50 mm at buckling to 72.6 mm (when unloading began) in approximately two minutes, compared to approximately 40 minutes to reach the buckling load. The bottom flange exhibited very limited lateral movement in comparison and moved in the opposite direction of the top flange. There is close to zero increase in vertical displacement after buckling, which differs slightly from previous studies (Fukumoto et al. 1980; Kabir and Bhowmick 2016) that show slight increase in vertical displacement even as the load drops; further attention to this behaviour will be noted in future tests. Similar to top flange lateral displacement, girder twist increases rapidly once the buckling load is attained. Though both top and bottom flange undergo large increases in twist, it is particularly pronounced in the top flange (maximum rotation of 9.05° compared to 6.25° in the bottom flange).

Table 4: Mid-span displacements and rotations at buckling vs. at maximum for SP2-2

	Top flange lateral (mm)	Bottom flange lateral (mm)	Bottom flange vertical (mm)	Top flange rotation (°)	Bottom flange rotation (°)
At Buckling	8.50	-0.80	55.3	0.86	0.82
At Maximum	72.6	-5.90	55.8	9.05	6.25

Fig. 9 shows the girder buckled towards the bottom left corner of the photo (westward in the laboratory); the load collar shown in the photograph is slightly different to the one presented in this paper as minor modifications have been made to the load collar since the first test.

Figure 9: Buckled SP2-2 at the end of the test

Using measured cross-section dimensions, mill test report yield strength of 386 MPa, and Eqs. 1-4, the CSA S16-14 predicted bending strength for SP2-2 is M_r = 2878 kN-m, which considers a resistance factor of ϕ = 1.0 and a moment distribution factor of ω_2 = 1.13. This corresponds to P_{avg} = 298 kN, which is a 19.6% difference compared to test results. However, CSA S16-14 assumes shear centre loading whereas the load height of the test is effectively 448 mm above the shear centre (i.e. 152 mm above the top flange), which has a destabilizing effect. This will considerably decrease moment capacity and will be accounted for in future evaluations of CSA S16-14's adequacy.

If the AISC Specification for Structural Steel buildings, ANSI/AISC 360 (AISC 2016), is used instead, the factored LTB strength for SP2-2 is calculated as per Eqs. 5-6:

$$M_c = \phi_b M_n \tag{5}$$

$$M_n = C_b \left[M_p - (M_p - 0.7 F_y S_x) \frac{L_b - L_p}{L_r - L_P} \right] \leq M_p \tag{6}$$

where M_c is the factored flexural strength, ϕ_b is the resistance factor for flexure, M_n is the nominal flexural strength, C_b is the LTB modification factor for non-uniform moment diagrams when both ends of the segment are braced, M_p is the plastic moment capacity of the section, F_y is the yield strength, S_x is the elastic section modulus about the x-axis, L_b is the length between points that are either braced against lateral displacement of the compression flange or braced against twist of the

cross-section, L_p is the limiting laterally unbraced length for the limit state of yielding, and L_r is the limiting unbraced length for the limit state of inelastic LTB.

Using ϕ_b=1.0 and a calculated C_b value of 1.14, AISC 360 yields a predicted flexural strength of M_c= 2967 kN-m, which is 3.1% larger than the CSA S16-14 prediction and a 22.0% difference compared to test results. However, like CSA S16-14, the AISC Specification assumes shear centre loading and therefore the predicted bending strength must be adjusted to account for load height.

5. Conclusions and future work

The successful testing of the first girder in the proposed lateral–torsional buckling test program is positive indication for the remaining tests. The results of the test program described herein amount to a significant contribution to available knowledge on the stability response of welded steel girders. The main findings of this study are summarized below:

- Finite element models of the test girders provided preliminary estimates of buckling load, displacements, and rotations to aid in the design of a test set-up, and particularly a loading mechanism that allows for the full range of movement expected in lateral–torsional buckling.
- The proposed test set-up and loading mechanism were able to properly simulate lateral–torsional buckling instability in the laboratory.
- Experimental lateral–torsional buckling moment was equal to 2313 kN-m, which is 19.6% and 22.0% lower than predictions from CSA S16 and AISC 360, respectively. However, the predicted capacities have not been adjusted to account for the effect of the load height.

The immediate upcoming research involves completion of physical testing to generate a larger database for evaluating the adequacy of CSA S16-14's lateral–torsional buckling provisions.

Acknowledgments

The authors gratefully acknowledge SSAB for their donation of plate material for girders; Supreme Group for fabrication of girders and ancillary testing fixtures; the financial assistance of NSERC; and the University of Alberta Steel Centre for challenging traditional boundaries of knowledge and research.

References

AISC. (2016). *ANSI/AISC 360-16 Specification for Structural Steel Buildings*. Chicago: American Institute of Steel Construction.

Ballio, G., Mazzolani, F. (2013). *Theory and Design of Steel Structures. Journal of Chemical Information and Modeling*. Vol. 53.

CSA. (2013a). *CSA G40.20-13/G40.21-13 General Requirements for Rolled or Welded Structural Quality Steel/Structural Quality Steel*. Missisauga: Canadian Standards Association.

———. (2013b). *W59-13 Welded Steel Construction (Metal Arc Welding)*. Missisauga: Canadian Standards Association.

———. (2014). *CAN/CSA-S16-14 Limit States Design of Steel Structures*. Toronto: Canadian Standards Association.

Dassault Systèmes. (2014). "Abaqus." Standard Version 6.14, Simulia Inc., Providence, RI, USA.

Fukumoto, Y. (1976). "Lateral buckling of welded beams and girders in HT 80 steel." *IABSE Congress Report*, 10: 403–408.

Fukumoto, Y., Itoh, Y., Kubo, M. (1980). "Strength variation of laterally unsupported beams." *ASCE Journal of Structural Division*, 106 (ST1) 165–81.

Fukumoto, Y., Kubo, M. (1977). "An Experimental Review of Lateral Buckling of Beams and Girders." *International Colloquium on Stability of Strucutres Under Static and Dynamic Loads*, 541–62. ASCE.

Galambos, T.V. (1977). "Laterally unsupported beams." *Second International Colloquium on Stability*, 365–73. Tokyo, Liege, Washington: European Convention for Constructional Steelwork.

Galambos, T.V. (1998). *Guide to Stability Design Criteria for Metal Structures*. 5th ed. New York: John Wiley & Sons, Inc.

Greiner, R., Kaim, P. (2001). "Comparison of LT-buckling design curves with test results." *European Convention for Constructional Steelwork*, ECCS TC 8 (23) 1–23. Brussels, Belgium.

Ji, X.L., Driver, R.G., Imanpour, A. (2018). "Lateral–torsional buckling response of welded wide-flange girders." *Proceedings of the Annual Stability Conference*, Baltimore, MD. 1–15. Structural Stability Research Council.

Kabir, I., Bhowmick, A.J. (2018). "Lateral torsional buckling of welded wide flange beams under constant moment." *Canadian Journal of Civil Engineering*, 45: 766–79.

Kabir, I., Bhowmick, A.J. (2016). "Lateral torsional buckling of welded wide flange beams." *M.A.Sc dissertation*, Department of Building, Civil and Environemntal Engineering, Concordia University. Montreal, QC.

MacPhedran, I., Grondin, G.Y. (2011). "A simple steel beam design curve." *Canadian Journal of Civil Engineering*, NRC Research Press, 38: 141–53.

Subramanian, L., White, D.W. (2017). "Resolving the disconnects between lateral torsional buckling experimental tests, test simulations and design strength equations." *Journal of Constructional Steel Research*, 128: 321–34.

Timoshenko, S.P., Gere, J.M. (1961). *Theory of Elastic Stability*. 2nd ed. New York: McGraw-Hill.

Unsworth, D.R., Li, L., Driver, R.G. (2019). "Lateral-torsional buckling in welded girders: prediction and measurement of residual stresses." *CSCE Annual Conference*, 1–10. Laval, QC. Canadian Society for Civil Engineering.

Yarimci, E., Yura, J.A., Lu, L.W. (1967). "Techniques for testing structures permitted to sway." *SESA Spring Meeting*, 1–11. Ottawa, ON.